ISSN: 2414-1895 DOI: 10.6919/ICJE.202603_12(3).0010

A Two-Stage Pre-Positioning Method for Resolver Zero-Offset Calibration in PMSM

Jiacheng Yao[a]

Xi'an Shiyou University, Xi'an 710065, China

[a]yokaseii@163.com

Abstract

High-performance control of Permanent Magnet Synchronous Motors (PMSMs) heavily relies on accurate rotor position information. However, the inherent zero-offset error in resolvers can lead to controller output disturbances and even induce significant safety hazards such as system shutdown. Therefore, this paper designs and implements a detection strategy for the zero-offset angle suitable for zero and low-speed operating conditions. To overcome the dead-zone issue in single pre-positioning at a power angle of π-where zero electromagnetic torque prevents rotor movement-a "two-stage pre-positioning" correction method is proposed. This approach implements an open-loop angle injection strategy. First, a 0° virtual angle and quadrature-axis current are injected for initial positioning. Then, the virtual angle steps to 90°, triggering a second positioning. This instantaneous 90° commutation of the stator field generates maximum transient torque, overcoming static friction and load torque to precisely align the rotor. Experiments validate that the proposed two-stage pre-positioning method safely and rapidly aligns the rotor to a determined position, enabling the acquisition of the actual zero-offset angle.

Keywords

PMSM; Zero-Offset Angle; Two-Stage Pre-Positioning.

1. Introduction

The ongoing evolution of industrial digitalization has cemented the role of Permanent Magnet Synchronous Motors as the core actuation units in modern servo systems. Within this context, the precision of initial rotor phase detection is a critical determinant of startup reliability. Inaccuracies in this phase can lead to a fundamental misalignment between the applied current vector and the actual rotor flux axis, resulting in suboptimal torque production, potential reverse rotation, and undue stress on the mechanical and electrical components, thereby compromising system longevity.

To address the challenge of zero-speed rotor position estimation, a variety of established techniques exist. Signal injection methods, such as those utilizing voltage pulses [1-2] or high-frequency carriers [3-5], exploit magnetic saliency to derive position information. While effective, these approaches can be computationally intensive or sensitive to parameter variations. Alternative strategies, like the one presented in [6], aim to simplify implementation by foregoing traditional PI regulators, while square-wave injection techniques [7-9] seek to enhance dynamic bandwidth. Despite their merits, many of these methods require complex signal processing.

This work proposes a practical and robust solution based on a modified pre-positioning framework. The conventional single-pulse pre-positioning method suffers from an inherent dead-zone when the initial rotor angle aligns at a power angle of π, where zero electromagnetic torque renders the rotor immovable. To overcome this fundamental limitation, we introduce a two-stage calibration technique.

ISSN: 2414-1895 DOI: 10.6919/ICJE.202603_12(3).0010

The proposed method operates by deliberately overriding standard closed-loop current control. An initial alignment is first enforced by injecting a zero-degree virtual angle alongside a quadrature-axis current. A subsequent, abrupt 90° step in the virtual angle is then commanded. This rapid reorientation of the stator magnetomotive force generates a peak transient torque impulse, sufficient to overcome static friction and load torques, thereby compelling the rotor to settle into a uniquely defined and accurate position. Experimental results confirm that this approach provides a reliable means to identify the true zero-offset angle quickly and safely, ensuring robust startup performance.

2. Principle of the Pre-Positioning Method

During the pre-positioning phase, a rotating reference frame dq is constructed based on the desired rotor position, while another rotating frame d*q* is established according to the actual rotor position. The angle between the q-axis and the d*-axis is defined as the power angle δ, as illustrated in Fig.1. A fixed current vector Is is applied to the motor stator windings. To maximize electromagnetic torque, this paper adopts id=0 vector control, meaning a stator current iq is applied along the q-axis, such that Is = iq. The component of iq projected onto the q*-axis generates electromagnetic torque that drives the rotor to rotate, ultimately causing the rotor to settle at the position corresponding to iq. The resolver's zero-offset angle Δθ0 is obtained by recording the actual position measured by the resolver at this point and calculating its deviation from the desired rotor position.

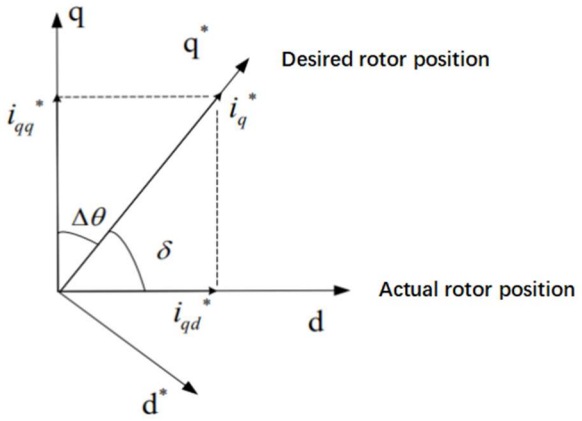

Fig. 1 Schematic diagram of pre-positioning method

Fig.1. demonstrates that during pre-positioning, due to the power angle δ, the stator current iq is resolved into two orthogonal components in the actual rotor d*q* frame-namely, iqq* along the q-axis and iqd along the d*-axis. The mathematical expression is given by:

$$\begin{cases} i_{qq*} = i_q \sin\delta \\ i_{qd*} = i_q \cos\delta \end{cases} \tag{1}$$

From the equation(1), the electromagnetic torque acting on the rotor can be expressed as:

$$T_e = 1.5 p_n i_{qq*} [\psi_f + (L_d - L_q) i_{qd*}] \tag{2}$$

Since the device under test in this experiment is a Surface-Mounted Permanent Magnet Synchronous Motor (SPMSM), whose dq-axis inductances are approximately equal, the reluctance torque arising from the inductance difference term can be neglected. The expression can thus be rewritten as:

ISSN: 2414-1895 DOI: 10.6919/ICJE.202603_12(3).0010

$$T_e \approx 1.5 p_n \psi_f i_{qq^*} = 1.5 p_n \psi_f i_q \sin\delta \tag{3}$$

Assuming the motor starts under no-load conditions, it can be seen from Equation (3) that as δ varies, Te changes accordingly, driving the rotor to rotate. The final stopping position of the rotor is shown in Fig.2. Where the desired rotor position corresponds to the q-axis.

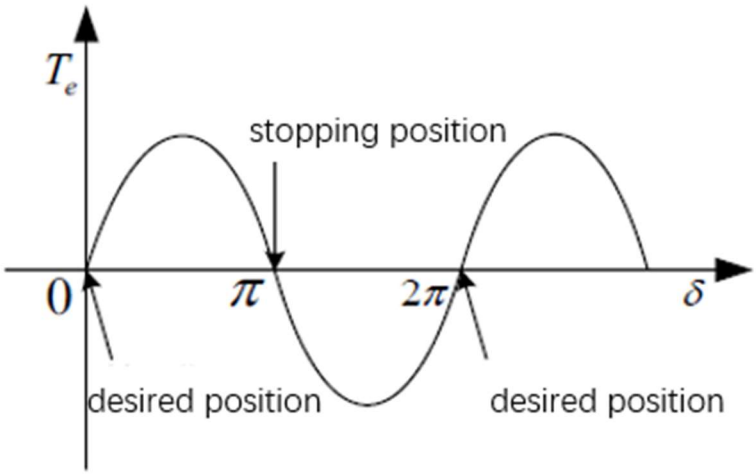

Fig. 2 Rotor position and power angle during first pre-positioning

As can be seen from Fig.2:When δ = 0, Te = 0, and the rotor settles on the q-axis. When 0 < δ < π, Te > 0, the rotor rotates counterclockwise and ultimately converges to the q-axis. When δ = π, Te = 0, the rotor cannot be driven and remains displaced by π from the q-axis. When π < δ < 2π, Te < 0, the rotor rotates clockwise and ultimately converges to the q-axis.

In particular, when δ = π, Te = 0, rendering the rotor immovable and preventing it from settling on the q-axis. To address this issue and avoid pre-positioning failure, a second pre-positioning procedure can be performed. It is sufficient to make the angle of the second pre-positioning differ by π/2 from that of the first, as illustrated in Fig.3. It can be observed that the new desired rotor position differs from the original desired position by π/2.

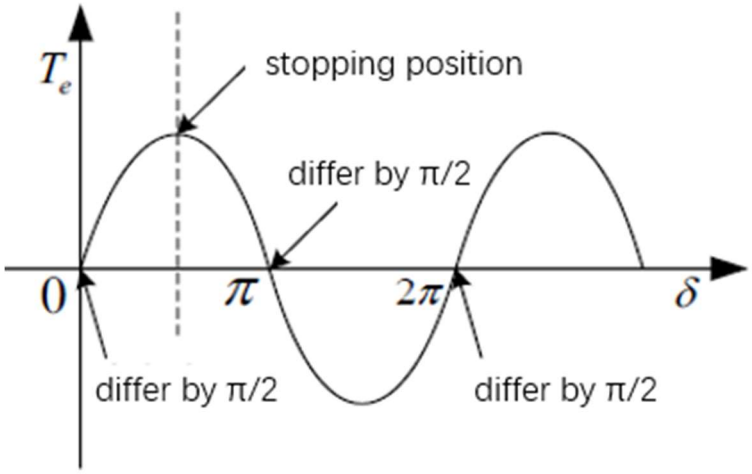

Fig. 3 Rotor position and power angle during second pre-positioning

ISSN: 2414-1895 DOI: 10.6919/ICJE.202603_12(3).0010

As shown in Fig.3, the rotor position that previously could not be driven (δ = π) now has an included angle of π/2 with the new desired rotor position. According to Equation (3), Te will reach its maximum value, enabling the rotor to be pulled to this new desired position. In cases where the first pre-positioning successfully dragged the rotor to the q-axis, the rotor is also offset by π/2 from the new desired rotor position. Ultimately, regardless of the initial condition, the rotor will be driven to converge at the new desired position.

Therefore, the two-stage pre-positioning method effectively avoids the positioning failure that occurs when δ = π, ultimately enabling the rotor to be aligned to the specified position.

3. Physical Implementation Logic

To map the aforementioned physical theory onto an actual embedded microprocessor, it is necessary to break the constraints of the conventional closed-loop control architecture and implement a software control strategy based on "open-loop angle injection."

Upon issuing the first pre-positioning command, the control system actively disconnects the feedback loop of the outer speed loop, retaining only the inner current loop for independent regulation. At the current loop reference input, the d-axis reference current is set to $i_d^* = 0$, while a constant q-axis reference current with amplitude I_{test} is applied as $i_q^* = I_{test}$. The most critical software modification lies in the controller's handling of position feedback: instead of utilizing the actual feedback angle θ_e obtained from the resolver-to-digital converter, a constant virtual electrical angle command $\theta_1^* = 0°$ is forcibly injected into the transformation matrices of both the Park and inverse Park coordinate transforms.

The virtual angle $\theta_1^* = 0°$ and reference current $i_q^* = I_{test}$ specified in the control software must ultimately be transformed into a physical stator magnetic field by the inverter hardware through Space Vector Pulse Width Modulation technology.

At the physical implementation level, since the coordinate transformation module continuously receives a constant virtual angle of 0°, the current loop PI regulators, after a brief transient adjustment, force the actual phase currents to converge to their constant references. Consequently, the output rotating-frame voltage references u_d^* and u_q^* also settle to DC constant values. As a result, the voltage components projected onto the two-phase stationary frame via the inverse Park transformation no longer appear as sinusoidal AC quantities typical of normal operation, but instead become DC constants, expressed as $u_\alpha = -u_q \sin\theta^*$ and $u_\beta = u_q \cos\theta^*$. Specifically, with an injection angle of 0°, the u_α component approaches zero, while the u_β component remains at its positive maximum value.

According to the space vector synthesis principle described in Chapter 2, when the reference voltage components input to the SVPWM module satisfy $u_\alpha = 0$ and $u_\beta > 0$, the target reference space voltage vector U_{out} aligns perfectly with the positive β-axis on the complex plane. Within the hexagonal space sector distribution of SVPWM, this target vector direction exactly bisects the boundary between Sector I and Sector II, namely bisecting the angle between the fundamental non-zero vectors $U_6(110)$ and $U_2(010)$. Consequently, when executing the seven-segment switching time allocation, the SVPWM algorithm evenly distributes the effective pulse width time between the fundamental vectors U_6 and U_2, while utilizing zero vectors to fill the remaining PWM switching cycles to ensure current continuity.

At the inverter hardware level, this configuration translates to continuous conduction of the B-phase upper switch (state 1) and C-phase lower switch (state 0) over successive switching cycles, while the A-phase leg switches with a 50% duty cycle (effectively outputting 0). This specific and constant switching state combination synthesizes a space voltage vector at the physical level that maintains constant amplitude and is rigidly locked along the stator β-axis direction. This stationary voltage vector, continuously applied to the three-phase stator windings, excites a stationary synthetic magnetic field in the air gap whose direction is "anchored" in mechanical position. The resulting

ISSN: 2414-1895 DOI: 10.6919/ICJE.202603_12(3).0010

traction electromagnetic torque forcibly "attracts" and pulls the rotor from its random initial position to the desired initial alignment position, thereby completing the first pre-positioning process.

At the software implementation level, the second pre-positioning does not alter the stator magnetic field intensity but instead relies on a transient jump in the field orientation. The control loop maintains completely constant current reference amplitudes with $i_d^* = 0$ and $i_q^* = I_{test}$, while applying a step change of $\pi/2$ to the virtual electrical angle command fed into the inverse Park transformation module, directly setting the new virtual positioning angle to $\theta_2^* = 90°$.

This seemingly simple step change in the variable triggers a dramatic transient response at the hardware level. Substituting into the inverse transformation matrix reveals that as the injection angle jumps to 90°, the stationary-frame voltage commands output by the inverse Park transform undergo an abrupt transition: the u_β component, previously maintained at its positive maximum value, instantly drops to zero, while the u_α component, previously zero, instantaneously jumps in the negative direction to its maximum amplitude. This means that the target reference space voltage vector U_{out} rotates counterclockwise by 90° on the complex plane, with its direction jumping directly from the positive β-axis to point toward the negative α-axis.

Referring to the SVPWM space voltage vector distribution diagram in Fig.4, the negative α-axis direction coincides exactly with the action axis of the fundamental non-zero voltage vector $U_3(011)$. Upon detecting this step change in the voltage command, the SVPWM modulation module rapidly abandons the previous switching time allocation scheme with microsecond-level response speed, instead allocating the entire effective action time to the new fundamental vector U_3. The underlying switching states of the inverter bridge subsequently undergo an abrupt transition: the A-phase lower switch remains continuously conducting (state 0), while the B-phase and C-phase upper switches remain continuously conducting (state 1).

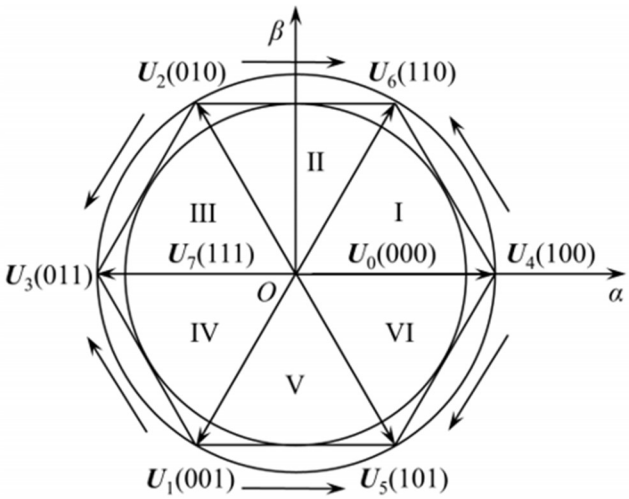

Fig. 4 Basic space voltage vector diagram

This instantaneous reconfiguration of the underlying PWM modulation state causes the stationary magnetic field excited by the inverter's three-phase output within the stator windings to abruptly jump by 90 electrical degrees. At the physical level, due to the mechanical inertia of the rotor, it cannot undergo any significant mechanical displacement during the extremely short transient period in which the stator magnetic field completes its electromagnetic transient. Consequently, an instantaneous electrical angle difference of $\pi/2$ is established between the rotor's actual flux axis and the new synthetic stator magnetic field axis. Substituting into the electromagnetic torque equation reveals that, since $\sin(\pi/2) = 1$, the system outputs the maximum transient electromagnetic torque reaching its theoretical peak at this instant, forcibly pulling the rotor into the new desired stable position.

ISSN: 2414-1895 DOI: 10.6919/ICJE.202603_12(3).0010

4. Experiments and Analysis of Results

To verify the effectiveness of the proposed model and method, an experimental platform was constructed as shown in Fig.5. The platform mainly consists of a DC power supply, a PMSM equipped with a resolver, a DSP28335-based development board, and a Raspberry Pi serving as the host computer. The host computer communicates with the development board primarily via CAN bus for data transmission. A detailed schematic of the system connections is shown in Fig.5.

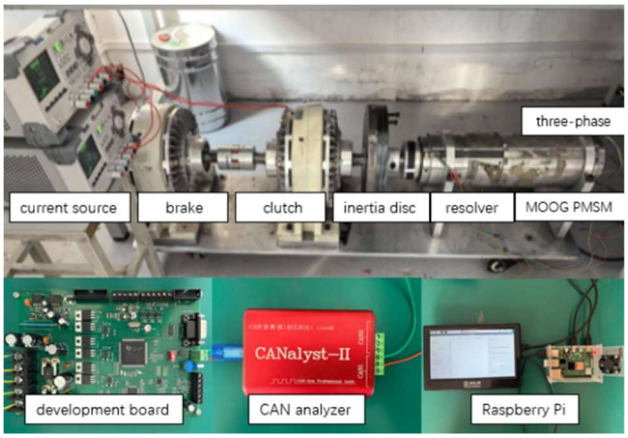

Fig. 5 Experiment platform

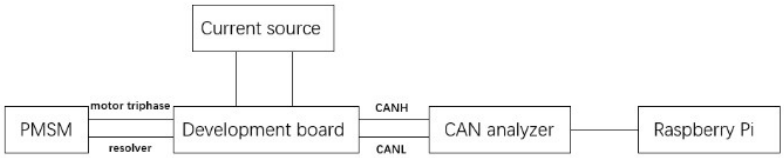

Fig. 6 Detailed schematic of the system connections

During the initial stage of the experiment, the control system injects a positioning current with a fixed direction into the stator and sets the virtual angle to 0°. As shown in Fig.7, the rotor is rapidly pulled from its random initial position of approximately 264° and converges within a very short time to the first steady-state plateau near 214°, where the rotor ceases rotation. Due to the inherent static friction torque and load torque present in the motor's physical system, a steady-state error exists between the actual stopping position and the ideal position.

To eliminate the potential risk that the first positioning might fall within the electromagnetic torque dead zone, the system triggers the second pre-positioning command at 1.75s, instantaneously stepping the virtual angle to 90°. As illustrated in Fig.7, at the moment the command is issued, the resolver feedback angle undergoes a steep jump, rapidly rising from approximately 214° and eventually stabilizing at a second steady-state plateau around 305°.

The significant angular jump of approximately 91° between the two steady-state plateaus validates that the 90° spatial commutation of the stator magnetic field effectively generates transient traction torque, completely overcoming the limitations of static friction torque. Experimental results demonstrate that this two-stage pre-positioning method can safely and quickly pull the rotor to a determined position.

ISSN: 2414-1895 DOI: 10.6919/ICJE.202603_12(3).0010

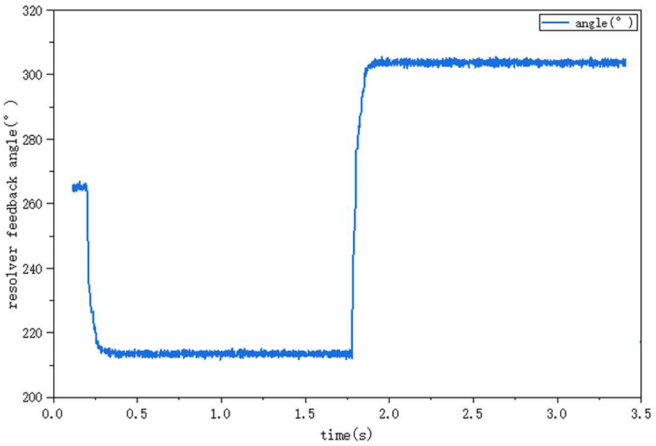

Fig. 7 Rotor position of pre-position

The calibrated rotor zero-position offset is transmitted to the entire motor control system. Once the motor receives a start command, the rotor speed begins to increase and eventually stabilizes at a preset value, as shown in Fig.8. This result demonstrates the accuracy of the zero-position offset obtained using the proposed method.

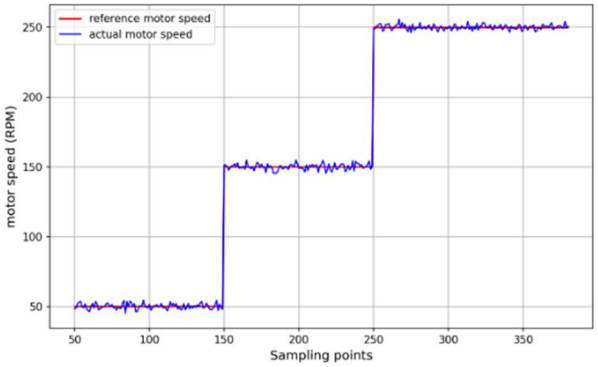

Fig. 8 Motor speed test diagram

5. Conclusion

This paper proposed a two-stage pre-positioning method based on open-loop angle injection to address the resolver zero-offset calibration issue in PMSM drives, specifically overcoming the dead-zone problem at power angle $\delta = \pi$ where conventional single pre-positioning fails. By sequentially injecting virtual electrical angles of 0° and 90° while maintaining constant q-axis current, the method achieves reliable rotor alignment: the first stage brings the rotor to an initial steady-state position, while the instantaneous 90° spatial commutation of the stator field in the second stage generates peak transient torque that overcomes static friction and load torque, ensuring convergence to a uniquely defined position regardless of initial conditions. Experimental results on a DSP28335-based platform validate that the two-stage approach produces an abrupt angular jump of approximately 91°, confirming effective transient torque generation, and the calibrated zero-offset angle enables stable motor startup and speed regulation. The method offers a hardware-efficient, computationally simple solution for robust initial rotor positioning in zero-speed applications.

References

[1] LIU Jilong, XIAO Fei, SHEN Yang. Positionsensorless control technology of permanent-magnet synchronous motor: A review[J]. Transactions of China Electrotechnical Society, 2017, 32(16): 76-88.

ISSN: 2414-1895 DOI: 10.6919/ICJE.202603_12(3).0010

[2] He Qianen, Lin Jianliaoyuan, Xu Xiuying. A novel method of angle sensor zero-position calibration based on line back-EMF for three-phase PMSM[J]. Journal of Chinese Inertial Technology, 2023, 31(04): 407-412.

[3] Zhang M, Guo C, Liang J. A high precision measurement method for zero position deviation of rotor position sensor of permanent magnet synchronous motor[J]. Microelectromechanics, 2016, 49(01): 40-43.

[4] Yang Luohong, Liu Kan, Hu Wei. A q-axis flux linkage identification based zero-correction for position sensor of permanent magnet synchronous motor[J]. Journal of Electrical Engineering, 2023, 17(4): 163-173.

[5] Wang Yaoqiang, Ma Xiaoyong, Cheng Zhiping. PMSM initial rotor position detection and startup strategy[J]. Electric Power Automation Equipment, 2016, 36(9): 156-161, 168.

[6] OH H, SONG K, CHO K. Initial rotor position detecting algorithm of PM synchronous motor using incremental encoder[C]//IEEE ECCE Asia Downunder, Melbourne, Australia, 2013:681-686.

[7] Li Yongqiang. Research on control method of high speed permanent magnet synchronous motor[D]. Hefei University of Technology, 2023.DOI:10.27101/d.cnki.ghfgu.2023.001320.

[8] Cao Hengpei, Ai Mengmeng, Wang Yanbo. Research status and development trend of permanent magnet assisted synchronous reluctance motor[J]. Transactions of China Electrotechnical Society, 2022, 37(18): 4575-4592.

[9] Sundararajan P, Sathik M H M, Sasongko F. Condition monitoring of DC-link capacitors using Goertzel algorithm for failure precursor parameter and temperature estimation[J]. IEEE Transactions on Power Electronics, 2020, 35(6): 6386-6396.